HHS Public Access

Author manuscript

Nat Metab. Author manuscript; available in PMC 2020 January 29.

Published in final edited form as:

Nat Metab. 2019 August ; 1(8): 765–774. doi:10.1038/s42255-019-0089-9.

m^{6}A mRNA Methylation Regulates Human β-Cell Biology in Physiological States and in Type 2 Diabetes

Dario F De Jesus[1,*], **Zijie Zhang**[2,3,*], **Sevim Kahraman**[1,*], **Natalie K Brown**[1], **Mengjie Chen**[4], **Jiang Hu**[1], **Manoj K Gupta**[1], **Chuan He**[2,3], **Rohit N Kulkarni**[1]

[1]Islet Cell and Regenerative Biology, Joslin Diabetes Center, Department of Medicine, Brigham and Women's Hospital, Harvard Stem Cell Institute, Harvard Medical School, Boston, MA 02215, USA.

[2]Department of Chemistry, Department of Biochemistry and Molecular Biology, and Institute for Biophysical Dynamics, The University of Chicago, Chicago, IL 60637, USA.

[3]Howard Hughes Medical Institute, The University of Chicago, Chicago, IL 60637, USA.

[4]Section of Genetic Medicine, Department of Medicine, Department of Human Genetics, The University of Chicago, Chicago, IL 60637, USA;

Abstract

The regulation of islet cell biology is critical for glucose homeostasis[1].N^6-methyladenosine (m^{6}A) is the most abundant internal messenger RNA (mRNA) modification in mammals[2]. Here we report that the m^{6}A landscape segregates human type 2 diabetes (T2D) islets from controls significantly better than the transcriptome and that m^{6}A is vital for β-cell biology. m^{6}A-sequencing in human T2D islets reveals several hypomethylated transcripts involved in cell-cycle progression, insulin secretion, and the Insulin/IGF1-AKT-PDX1 pathway. Depletion of m^{6}A levels in EndoC-βH1 induces cell-cycle arrest and impairs insulin secretion by decreasing AKT phosphorylation and PDX1 protein levels. β-cell specific Mettl14 knock-out mice, which display reduced m^{6}A levels, mimic the islet phenotype in human T2D with early diabetes onset and mortality due to decreased β-cell proliferation and insulin degranulation. Our data underscore the significance of RNA methylation in regulating human β-cell biology, and provide a rationale for potential therapeutic targeting of m^{6}A modulators to preserve β-cell survival and function in diabetes.

Correspondence to: Rohit N. Kulkarni M.D., Ph.D., Islet Cell and Regenerative Biology, Joslin Diabetes Center, One Joslin Place, Boston, 02215 MA, Tel: +1-617-309-3460 – Fax: +1-617-309-3476, Rohit.Kulkarni@joslin.harvard.edu, Chuan He Ph.D., Department of Chemistry, The University of Chicago, 929 E. 57th St., Chicago, 60637 IL, Tel: +1-773-702-5061 -Fax: +1-773-702-0805, chuanhe@uchicago.edu.

AUTHOR CONTRIBUTIONS

DFDJ conceived the idea, designed and performed the experiments, analyzed the data and wrote the manuscript. ZZ designed and performed the experiments, analyzed the data and wrote the manuscript. SK performed cell culture experiments and analyzed the data. NKB performed morphometric analyses of pancreases. JH performed immunohistochemistry. MKG performed RT-PCRs. CH contributed to conceptual discussions and designed the experiments. RNK contributed to conceptual discussions, designed the experiments, supervised the project and wrote the manuscript. All the authors have reviewed, commented and edited the manuscript.

*These authors contributed equally to this work.

COMPETING FINANCIAL INTERESTS

C.H. is a scientific founder and a member of the scientific advisory board of Accent Therapeutics Inc. The remaining authors have no conflicts of interest.

To determine if m^{6}A regulators are expressed in human pancreatic β-cells, we undertook immunofluorescence analyses of human pancreatic sections obtained from non-diabetic (control) individuals. We detected abundant protein levels of the m^{6}A writers, METTL3, METTL14 and the eraser alkB homolog 5 (ALKBH5) (Supplementary Figure 1a). These data, together with a study reporting the expression of fat mass and obesity–associated gene (FTO)[3] in β-cells, provide evidence for the presence of m^{6}A mediators in human islets. Then, we asked if the expression of m^{6}A modulators is altered in T2D. Re-analyses of a publicly available dataset on single-cell RNA-sequencing (GSE81608), comparing controls to T2D human dispersed islets[4], revealed that several m^{6}A modulators were down-regulated in β-cells in T2D (Supplementary Figure 1b). In contrast, α-cells showed either no alteration or changes that trended in the same direction as in β-cells (Supplementary Figure 1b). In β-cells, this analysis revealed downregulation of *METTL3*, *ALKBH5*, and *YTHDF1* (Supplementary Figure 1c). Indeed, mRNA analyses of whole islets collected from controls and T2D patients also revealed a generalized downregulation of several m^{6}A modulators (Supplementary Figure 1d). Furthermore, METTL3 and METTL14 protein levels were decreased in whole islets from T2D patients which also expressed low levels of PDX1 compared to controls (Supplementary Figure 1e,f). Together, these data revealed that m^{6}A modulators are detectable in human β-cells and are particularly affected by T2D in comparison to other islet cell types.

Next, we compared m^{6}A-sequencing versus RNA-sequencing in human islets obtained from controls and T2D patients (Supplementary Table 1) using previously described methods[5] (see methods). While RNA-sequencing was able to segregate samples by disease status there was considerable variability that limited the ability to identify differential gene expression among these samples (Figure 1a,b). A lack of statistical power in transcriptomic analyses due to high sample variability has been recognized to directly impact the ability to detect differentially expressed genes in studies using human islets and has necessitated employing large sample numbers[6]. Recently, single-cell RNA-sequencing studies comparing human islets from non-diabetic controls versus T2D patients have revealed altered expression in less than 0.5% of all detected genes[7]. Nevertheless, we did observe alterations in the islet transcriptome including genes (Supplementary Figure 2a) and pathways (Supplementary Figure 2b,c and Supplementary Dataset 1) associated with the disease. Examples of up-regulated genes (Supplementary Figure 2d) included *FGF2* which has been recently linked to β-cell dedifferentiation[8], while down-regulated genes (Supplementary Figure 2e) included *GLUT2* (*SLC2A2*) that is important in glucose-stimulated insulin secretion (GSIS)[9].

In contrast to the transcriptome, the m^{6}A methylome clearly segregated disease status in a relatively homogeneous manner in T2D samples (Figure 1c,d). To test if the m^{6}A methylome correlates with gene expression in T2D, we assessed the variability of gene expression at single-cell level specifically in β-cells from single-cell RNA sequencing in dispersed islets from controls and T2D humans (GSE81608)[4] and stratified m^{6}A genes based on our m^{6}A-seq data. m^{6}A genes presented significantly higher variability compared to non-m^{6}A, and within the m^{6}A genes the coefficient of variation was higher in T2D as compared to controls (Figure 1e), suggesting a higher impact of m^{6}A on the dynamic regulation of β-cell gene expression in T2D. Differential analysis of m^{6}A-sequencing revealed 6,078 differently methylated sites in 4,155 genes (FDR<0.05) and a higher number

of sites with decreased levels of m^{6}A methylation in T2D compared to controls (Figure 1f). Consistent with previous studies[5,10], m^{6}A peaks were enriched at the start and stop codons (Supplementary Figure 3a,b) and were characterized by the canonical GGACU motif (Supplementary Figure 3c). Gene ontology (GO) analyses of the m^{6}A methylome revealed that the genes affected in T2D involved cell-cycle, receptor signaling, insulin secretion and pancreas development (Figure 1g and Supplementary Dataset 2). Further pathway analyses of transcripts affected by m^{6}A hypomethylation revealed several networks important for β-cell biology and associated with diabetes development (Supplementary Figure 4a) including maturity-onset diabetes of the young (MODY) (Supplementary Figure 4b) and insulin/insulin-like growth factor receptor (IGF1R) signaling (Supplementary Figure 4c). More specifically, the Insulin/IGF1 -AKT-PDX1 pathway was significantly affected by hypomethylation in T2D (Figure 1h) highlighted by the genes in this pathway including *PDX1*, *IGF1R*, *TRIB3*, and *PPP3CA* (Figure 1i and Supplementary Figure 4d-m). Indeed, impairment in Insulin/IGF1-AKT signaling followed by down-regulation of PDX1 is a recognized mechanism associated with T2D[11–15]. While AKT promotes cell survival, growth and protein stability of PDX1[14,15] itself, the latter regulates β-cell identity, cell-cycle, and proper insulin secretion[12–15]. Together, these data prompted us to hypothesize that hypomethylation seen in T2D islets leads to cell-cycle arrest and impaired insulin secretion through down-regulation of Insulin/IGF1-AKT-PDX1 pathway.

To test this, we knocked-down (KD) METTL3 or METTL14 in the human β-cell line EndoC-βH1 followed by m^{6}A and RNA-sequencing. EndoC-βH1 cells express key β-cell genes such as PDX1[16,17] and are generally accepted as a model of human β-cells. METTL3 KD or METTL14 KD was each efficient (Supplementary Figure 5a,b) and did not significantly affect the mRNA levels of the YTH family m^{6}A readers (Supplementary Figure 5c). Differentially expressed genes (DEGs) induced by METTL3 KD or METTL14 KD were likely m^{6}A-mediated as shown by a strong positive correlation between common DEGs (Supplementary Figure 5d). As expected, peak calling revealed m^{6}A peaks in both groups enriched at the start and stop codons (Supplementary Figure 5e). Consistent with our hypothesis, transient ablation of m^{6}A in EndoC-βH1 cells was sufficient to induce G0-G1 cell-cycle arrest (Supplementary Figure 6a,b), and activation of the ATM-dependent DNA damage response (Supplementary Figure 6c,d). Ablation of METTL3 or METTL14 in dispersed human islet cells (Supplementary Figure 7a) confirmed up-regulation of the genes involved in cell-cycle arrest (Supplementary 7b). Furthermore, METTL3 KD and METTL14 KD in EndoC-βH1 cells each resulted in increased basal insulin secretion (Supplementary Figure 8a), impaired GSIS (Supplementary Figure 8a,b) and decreased insulin content (Supplementary Figure 8c). Congruently, RNA-sequencing (Supplementary Figure 9a,b and Supplementary Dataset 3) and m^{6}A-sequencing (Supplementary Figure 10a,b and Supplementary Dataset 4) analyses revealed that METTL3 KD and METTL14 KD altered the expression and methylation of transcripts involved in cell-cycle and insulin secretion.

To further confirm the role of m^{6}A in modulating T2D β-cell pathophysiology, we intersected DEGs in METTL3 KD or METTL14 KD datasets (FDR<0.10), obtained from a homogeneous and β-cell specific system (e.g. EndoC-βH1 cells), with m^{6}A-sequencing data obtained from islets of T2D patient samples (FDR<0.01) (Figure 2a). This intersection identified 475 differently methylated and expressed genes that were also enriched for cell-

cycle and insulin secretion processes (Figure 2b, Supplementary Figure 11a and Supplementary Dataset 5) and involved several candidates in the Insulin/IGF1-AKT-PDX1 pathway (Supplementary Figure 11a-e and Supplementary Dataset 5). This supported our previous findings and validated our KD system as a suitable model to mimic T2D in a β-cell specific manner. Next, we explored the effects of m^{6}A ablation on the β-cell response to stimulation with exogenous insulin or IGF1. First, to assess if m^{6}A modulates the IGF1>AKT signaling axis we stimulated METTL3 KD or METTL14 KD EndoC-βH1 cells with exogenous IGF1. Cells with a KD of either METTL3 or METTL14, when compared to scramble, exhibited decreased phosphorylation of IR/IGF1R and AKT (serine 473 and threonine 308 in METTL3 KD) (Figure 2c-f). Second, we asked if insulin>AKT signaling is also affected by m^{6}A depletion. Consistently, insulin stimulation of METTL3 KD or METTL14 KD resulted in a drastic decrement of AKT phosphorylation (s473 and t308) as compared to scramble (Figure 2g-j). Finally, because the protein level of PDX1 is known to be regulated in an AKT-dependent manner[18] and m^{6}A has been reported to affect translation of m^{6}A-methylated transcripts[19], we hypothesized that m^{6}A hypomethylation affects PDX1 protein expression. To test this, we generated stable METTL3 KD, METTL14 KD and METTL3/14 (METTL3 plus METTL14) KD EndoC-βH1 cells. Indeed, a reduction in PDX1 m^{6}A level was observed upon METTL3 KD or METTL14 KD (Figure 2k), consistent with the hypomethylation observed in islets from T2D patients (Figure 1i). A consistent downregulation of PDX1 protein levels was also observed upon METTL3 KD or METTL14 KD (Figure 2l-m). Cells with a stable KD of METTL14 exhibited a drastic downregulation of PDX1 protein abundance (Figure 2l-m), however, the consequent reduced proliferation presented a challenge to expand the cell colonies. Therefore, to further investigate the involvement of AKT in the modulation of PDX1 levels and dissect the direct impact of m^{6}A in controlling PDX1 translation we chose to treat scramble and stable METTL3 KD cells with an AKT agonist (SC79) or DMSO for 48 h. SC79 is known to increase AKT phosphorylation (t308 and s473) that is evident up to ~6h followed by progressive downregulation to basal levels[20]. However, the effects on protein synthesis last at least 48h[20]. In our studies, SC79 increased PDX1 protein levels in scramble cells, however, METTL3 silencing blocked the increase suggesting that m^{6}A regulates PDX1 protein levels synergistically with AKT in an independent pathway such as by modulating translation efficiency (Figure 2n,o). Other potential mechanisms that regulate PDX1, independent of changes in m^{6}A, warrant further investigation. Together these data point to a role for m^{6}A in modulating the insulin/IGF1-AKT-PDX1 signaling axis to regulate cell-cycle and insulin secretion in β-cells.

Finally, to validate our findings in an *in vivo* mammalian system we generated Mettl14 β-cell specific knock-out mice (M14KO) (Supplementary Figure 12a-d). M14KO mice were born in a normal Mendelian ratio and presented normal body weight trajectories until 3 months of age when they became severely polyuric, polydipsic, and showed weight loss (Figure 3a). Random-fed blood glucose levels were elevated at 1 month of age and worsened by 3 months (Figure 3b). Severe glucose intolerance (Figure 3c) was likely due to impaired GSIS *in vivo* (Figure 3d,e) without changes in insulin sensitivity (Figure 3f). Males and females presented similar phenotypes and died ~4–5 months of age due to severe diabetes. Further investigation of M14KOs revealed decreased β-cell mass starting at ~2 months of

age (Figure 3g,h, and Supplementary Figure 12e), largely secondary to impaired β-cell proliferation (Figure 3i,j) and minimally due to increased apoptosis (Supplementary Figure 12f). A gradual loss of Pdx1+/ins+ cells with age was consistent with loss of β-cell identity in the M14KO group (Figure 3k,l). Electron-microscopic analyses of M14KO β-cells revealed severe insulin degranulation accompanied by nuclear membrane stretching and enlarged mitochondria characteristic of cellular stress[21] (Figure 3m). Gene expression analyses in islets from 2-month-old M14KOs compared to controls revealed down-regulation of key cell-cycle genes (*Ccnd1*, *Ccnd2*, *Cdk4*) and increased expression of the cyclin-dependent kinase inhibitor *p21* (Figure 3n) consistent with G0-G1 cell-cycle arrest. The M14KOs also exhibited changes in β-cell identity and increased expression of early β-cell development markers (*Hnf1a*, *Hnf4a*, *Nkx6.1*) while showing decreased expression of mature β-cell markers such as *Pdx1*, *Mafa*, *and Ucn3* (Figure 3n). Finally, to confirm the involvement of Insulin/IGF1-AKT-PDX1 pathway in these effects, we collected primary islets isolated from 8 week-old male controls and M14KOs and analyzed candidate proteins that showed hypomethylation in human T2D (Figure 1h). M14KOs showed decreased protein levels of Igf1r and increased abundance of two negative modulators of AKT signaling, namely, calcineurin A (PP2BA) and Shp-2 (Figure 3o,p). These changes were accompanied by a robust reduction in Akt phosphorylation and Pdx1 protein levels (Figure 3o,p).

To further validate the transcriptomic changes driven by Mettl14 deficiency in β-cells, we collected FACS sorted β-cells[22] (Supplementary Figure 12g) from 6 week-old male mice for RNA-sequencing (Figure 4a). Enriched pathway analyses of differentially expressed genes (FDR<0.10) revealed PI3K-AKT, type 2 diabetes, insulin secretion and MODY pathways (Figure 4b and Supplementary Dataset 6). In particular, *Mettl14* KO resulted in down-regulation of G0-G1 cell-cycle progression mediators including *Ccnd1*, *Ccnd2*, and *Cdk4* (Figure 4c). Furthermore, m^6A deficiency resulted in down-regulation of *Igf1r*, *Slc2a2* and several β-cell identity genes including *Nkx6–1*, *Mafa* and *Pax6* (Figure 4c). On the other hand, M14KO β-cells presented increased expression of genes involved in autophagy (e.g. *Atg4b*), apoptosis (e.g. *Bcl2*) and negative regulation of AKT (e.g. *Ptpn13*) (Figure 4c).

To gain insights into the role of m^6A in regulating the IGF1/insulin>AKT>PDX1 pathway and to dissect the signaling networks modulating AKT phosphorylation we subjected islets from control and M14KO mice to phospho-antibody microarrays (Figure 4d). Pathway analyses of differentially phosphorylated proteins revealed insulin, PI3K-AKT, cell-cycle, and IGF1R signaling (Figure 4e and Supplementary Dataset 7). Notably, AKT modulators, whose activities were among the most impacted by Metl14 KO, included Erb-B2 receptor tyrosine kinase 3 (Errb3_Y1328) and Pten (Pten_S380, T382, S358) (Figure 4f). Errb3 is a tyrosine kinase receptor that forms a complex with p85 (PI3K) and Src, and is critical for activation of the PI3K-AKT signaling pathways[23]. Errb3 phosphorylation is severely down-regulated in M14KO islets consistent with decreased AKT activation. The phosphatase Pten, negatively regulates PI3K and inhibits AKT phosphorylation[24], and is negatively regulated by phosphorylation of its 3 tail residues (S380, T382, and T383)[25]. Pten phosphorylation was reduced in M14KO islets consistent with increased phosphatase activity and consequently downregulation of AKT phosphorylation. Finally, we used STRING[26] to construct a functional protein-protein interaction network (Figure 4g and Supplementary

Dataset 8). This analysis identified two main nodes involving AKT (Figure 4g, red spheres) and cell-cycle (Figure 4g, green spheres), depicting the central interactions between AKT, IGF1R, and PTEN to regulate cell-cycle progression.

Overall, our study demonstrates that m^{6}A methylation controls the Insulin/IGF1-AKT-PDX1 pathway. We confirmed that ablation of m^{6}A levels by targeting METTL3 or METTL14 recapitulates human T2D by decreasing AKT phosphorylation and PDX1 protein levels, resulting in cell-cycle arrest and impaired GSIS (Figure 4h). Further studies are needed to elucidate if hypomethylation seen in T2D is locus specific or if they result from a global reduction in the m^{6}A levels.

In summary, we observed that mRNA m^{6}A methylation is a much better mark than mRNA level to segregate human T2D islets from controls, suggesting that mRNA m^{6}A methylation contributes significantly to the pathogenesis of T2D. In general, we observed reduced overall m^{6}A methylation on key transcripts in T2D versus controls, which is consistent with the down-regulation of methylation components in T2D patients. Studies to date have focused on RNA m^{6}A methylation as a critical mechanism to regulate cell differentiation and development[2] in hematopoietic cells[27] and neurons[28]. Reduced global methylation occurs at the cell differentiation stage, and certain cancers hijack reduced RNA methylation to gain proliferation advantages[29]. Studies also suggest that aging correlates with noticeably reduced global m^{6}A methylation[30]. Together with previous reports, our data suggest that proper RNA m^{6}A methylation is critical to maintaining healthy cells with broad implications for metabolic tissues. We propose that reduced RNA methylation in key β-cell genes is a significant contributor to the pathophysiology of human T2D. We suggest that therapeutic targeting of regulators of m^{6}A in a β-cell specific manner in combination with current therapeutic agents might be a new avenue to counter the decreased m^{6}A levels in T2D islets and to promote β-cell survival and function.

METHODS

Human islet isolation and processing

Human islets were obtained from the Integrated Islet Distribution Program (IIDP) and Prodo Laboratories. Upon receipt, islets were cultured overnight (16h) in Miami Media #1A (Cellgro, USA). Islets were then handpicked, washed 2 times by self-sedimentation with ice-cold Dulbecco's phosphate buffered saline (DPBS) and 20,000 islets equivalents (IE) were pelleted for RNA isolation.

Mouse studies

Mettl14$^{fl/fl}$ mice on a C57BL/6N background were crossed with B6(Cg)-Ins1tm1.1(cre)Thor/J[31] (Jackson Labs, USA) mice, that did not harbor the nicotinamide nucleotide transhydrogenase (Nnt) mutation, to generate the knockouts. Mice were weaned at 3 weeks of age and maintained on chow diet (PicoLab® mouse diet 20 – 5058). Mice were anesthetized using Avertin and blood was collected by heart puncture from all the animals used in our experiments unless otherwise specified. Serum insulin and c-peptide levels were measured using ELISA kits (Crystal Chem., USA) according to manufacturer

guidelines. Littermate controls were always used and no animals were excluded from our studies. Sample sizes for animal experiments were chosen on the basis of experience in previous in-house studies[32–36] of metabolic phenotypes and to balance the ability to detect significant differences with minimization of the numbers of animals used in accordance with NIH guidelines.

Intraperitoneal glucose tolerance test (GTT), insulin tolerance test (ITT) and *in vivo* glucose-stimulated insulin secretion (GSIS) assays

For the glucose-tolerance tests, animals were fasted for 16h O/N and 20% (v/v) dextrose (Hospira, USA) was injected via the intraperitoneal (I.P.) route (2g/kg body weight). Blood glucose levels were measured using an automated glucose monitor (Glucometer Elite, Bayer, Germany) by tail puncture immediately before and at 15, 30, 60 and 120 minutes after injection. For the *in-vivo* glucose-stimulated insulin secretion mice were fasted for 16h O/N and 20% (v/v) dextrose (Bioexpress, USA) was injected via the I.P. route (3g/kg body weight). Serum was collected by tail vein at minutes 0, 2 and 5 after injection and insulin was assayed with an insulin ELISA kit (Crystal Chem., USA) according to manufacturer instructions. The insulin-tolerance test was performed after fasting animals for 5h and 0.75 U/kg insulin (Humalog, USA) was administered I.P. Glucose levels were measured using an automated glucose monitor by tail punch at time points 0, 15, 30 and 60 minutes after injection and were plotted with reference to the initial glucose levels.

Mouse Islet Isolations

Islet isolations were performed in anesthetized mice and their pancreas infused with liberase (Roche, Germany). Following incubation at 37°C for 17 min the digested pancreases were washed filtered through a 400μm filter and run on a Histopaque (Sigma, USA) gradient[36]. The purified islets were handpicked, counted and cultured overnight in 7mM glucose RPMI media (Gibco, USA) containing 10% FBS and 1% penicillin-streptomycin (PS) (Gibco, USA). Islets were handpicked, washed 2 times with ice-cold DPBS by self-sedimentation and used for experiments.

β-cell sorting by FACS

Overnight cultured mouse islets from control and M14KO mice were dispersed by treating with a solution of 1 mg/ml trypsin (Sigma, USA) and 30 μg/ml DNase (Roche, Germany) followed by incubation for 15 min in a 37°C incubator. During the digestion, the islets were vortexed every 5 min for 10s. Cold media containing serum was added to stop the digestion, and the cells were washed 2 times in DPBS containing 1% fatty-acid-free bovine serum albumin (BSA; Roche, Germany). Before sorting, islet cells were filtered through a 35 μm filter and sorted using MoFlo Cytometer (Dako, USA), where cells were gated according to forward scatter and then sorted on the basis of endogenous fluorescence[22,35] (for gating strategy please consult Reporting Summary).

Pancreas immunostaining and analyses

Mouse pancreas was collected and fixed in 4% formaldehyde at 4°C overnight, followed by paraffin embedding. Five-micron thick slides were cut and subjected to immunostaining.

Slides were heated in 10mM sodium citrate, followed by blocking with donkey serum and incubated with various primary antibodies: Ki67 (#550609, BD, USA), Anti-METTL3 (#195352, Abcam, USA), Anti-METTL14 (#HPA038002, Sigma, USA), ALKBH5 (#HPA007196, Sigma, USA), PDX1 (#5679, Cell Signaling, USA), Insulin (#ab7842, abcam, USA), Glucagon (#G2654, Sigma, USA), Somatostatin (#ab64053, abcam, USA). Specific signal was detected by using fluorescence-conjugated secondary antibodies (Jackson Immunoresearch, Alexa 488, Alexa 594, and AMCA) (please see Reporting Summary for details on antibodies used). Images were captured using Zeiss Axio Imager A2 upright fluorescence microscope. The β-cell mass was calculated by generating the ratio of the cross-sectional area of total number of pixels of insulin positive cells to the cross-sectional area of total number of pixels of the pancreatic tissue, multiplied by the pancreas weight of the mouse. We evaluated β-cell proliferation by co-immunostaining one section of each pancreas sample with Ki67, insulin and DAPI and counting 1000–2000 cells in a blinded manner by a single observer[33,34,37].

EndoC-βH1 Cell Culture

Culture flask were coated with DMEM (glucose 4.5 g/L; Gibco, USA) containing PS (1%; Gibco, USA), fibronectin (2 μg/mL; Gibco, USA), and extracellular matrix (1% vol/vol; Sigma, USA) and incubated for at least 1h in 5% CO_2 at 37°C before the cells were seeded. EndoC-βH1 cells were grown on Matrigel/fibronectin-coated culture flasks containing DMEM (glucose 1 g/L), BSA fraction V (2% wt/vol) (Roche, Germany), 2-mercaptoethanol (50 μM; Sigma, USA), nicotinamide (10 mM; Sigma, USA), transferrin (5.5 μg/mL; Sigma, USA), sodium selenite (6.7 ng/mL; Sigma, USA), PS (1%)[16].

Transfection knock-downs

Transient knock-downs—Reverse transfections were performed by mixing cells with Lipofectamine RNAiMAX Reagent (Life Technologies, USA) and small interfering RNA complexes (Dharmacon, USA) at a final concentration of 10 nmol/L siRNA according to manufacturer instructions. The cells were seeded at a density of 6×10^4 cells/cm^2. siGLO Red Transfection Indicator D-001630-02-05; siGENOME Non-Targeting siRNA Pool #1 D-001206-13-05, siGENOME METTL14 siRNA M-014169-00-0005; and siGENOME METTL3 siRNA M-005170-01-0005 (Dharmacon, USA) were used.

Stable knock-downs—EndoC-βH1 cells were transduced using high titer lentiviral particles in the presence of 10 μg/ml polybrene. SMARTvector Human lentiviral vectors containing shRNAs targeting METTL3 (cat# V3SH7590–226890163) or METTL14 (cat# V3SH7590–224822755) were purchased from Dharmacon, USA. Non-targeting Control lentiviral particles were used as scramble control (cat#S09-005000-01). Puromycin (2 μg/ml) was added to the culture media starting from post-transduction day 4 to select stable knock-down cells.

Insulin secretion assay

EndoC-βH1 cells were starved overnight in 2.8 mM glucose containing DMEM growth media followed by 1h in Krebs Ringer Buffer (KRB) containing NaCl (115 mM), $NaHCO_3$ (24 mM), KCl (5 mM), $MgCl_2$ (1 mM), $CaCl_2$ (1 mM), HEPES (10 mM), BSA (0.2% wt/

vol), 0.5 mM glucose. Static insulin secretion assays were then initiated by adding KRB containing 3.3 mM or 16.7 mM glucose for 1 hour. Aliquots of supernatants were removed, centrifuged to discard dead cells and stored for analysis in ice-cold acid ethanol that was added to extract insulin content from cells. Insulin secretion and content were measured by the human insulin ELISA (Mercodia, USA) according to the manufacturer's instructions.

Cell cycle analysis

EndoC-βH1 cells were trypsinized, washed with DPBS, and fixed with 70% ethanol. Fixed cells pelleted, resuspended in PBS containing 0.5 mg/ml RNase A (Sigma, USA), and incubated at 37°C for 1 hour. Ten μg/ml propidium iodide (Sigma, USA) was added and cells were filtered through a 30 μm nylon mesh and analyzed by LSRII (Joslin Flow Cytometry Core) (for gating strategy please consult reporting summary).

Insulin/IGF-1 stimulation

For exogenous insulin/IGF-1 treatment, EndoC-βH1 cells were transfected and starved overnight in 2.8 mM glucose containing DMEM growth media 48 h after transfection. Cells were further incubated for 1h in glucose-free DMEM media with 0.1% fatty acids free bovine serum albumin (BSA), followed by stimulation with insulin (100 nM) or IGF-1 (100 nM) (Sigma, USA) for 15 minutes.

SC79 treatment

Scramble and METTL3 stable knockdown cells were seeded in 6 well plates at a density of 6×10^4 cells/cm^2. There days after seeding, DMSO or SC79 (8 μg/mL; Selleckchem, USA) was added to the culture medium for 48 h. Cells were washed with DPBS and pelleted for protein isolation and western-blotting.

RNA isolation and RT-PCRs

High-quality total RNA (>200nt) was extracted using standard Trizol reagent (Invitrogen, USA) according to manufacturer instructions and the resultant aqueous phase was mixed (1:1) with 70% RNA-free ethanol and added to Qiagen Rneasy mini kit columns (Qiagen, Germany) and the kit protocol was followed. The RNA quality and quantity were analyzed using Nanodrop 1000 and used for reverse transcription using the high-capacity cDNA synthesis kit (Applied Biosciences, USA). cDNA was analyzed using the ABI 7900HT system (Applied Biosciences, USA) and gene expression was calculated using the $^{\Delta\Delta}$Ct method. Data were normalized to β-actin (please consult Supplementary Table 2 for primer sequences).

Protein isolation and Western-blotting

Total proteins were harvested from tissue and cell lines lysates using M-PER protein extraction reagent (Thermo Fisher, USA) respectively supplemented with proteinase and phosphatase inhibitors (Sigma, USA) according to standard protocol. Protein concentrations were determined using the BCA method followed by standard western immunoblotting of proteins using different primary antibodies: Anti-METTL3 (#195352, abcam, USA), Anti-METTL14 (#HPA038002, Sigma, USA), Anti-FTO (#ab124892, abcam, USA), Anti-P21

(#ab109199, abcam, USA), Anti-Phospho-AKT (#9271, Cell Signaling, USA), Anti-AKT (#9272, Cell Signaling, USA), Anti-Phospho ATM (#4526, Cell Signaling, USA), Anti-ATM (#2873, Cell Signaling, USA), Anti-Phospho-IR/IGF1R (#3021, Cell Signaling, USA), Anti-IGF1Rβ (#9750, Cell Signaling, USA), Anti-IRβ (#3025, Cell Signaling, USA), Anti-PDX1 (#5579, Cell Signaling, USA), Anti-Pan-Calcineurin A (#2614, Cell Signaling, USA), Anti-SHP-2 (#3397, Cell Signaling, USA), Anti-β-Actin (#4970, Cell Signaling, USA), Anti-αTubulin (#7291, abcam, USA). (Please see Reporting Summary for further details on antibodies used). The blots were developed using chemiluminescent substrate ECL (ThermoFisher, USA) and quantified using Image studio Lite Ver. 5.2 software (LICOR, USA).

m^{6}A immunoprecipitation and sequencing

To profile the m^{6}A methylome of the T2D islets, we applied m6A-seq (m6A-MeRIP-seq) to 7 T2D patients and 8 non-diabetic controls as well as one prediabetic sample and one sample from an adolescent non-diabetic. A minimum of 20,000 human islets equivalents (IEQs)/patient were used for total RNA extraction using Trizol according to the manufacturer's instruction. mRNA was isolated from total RNA using Dynabeads mRNA DIRECT purification kit (Thermo Fisher, USA). mRNA was adjusted to 15ng/ul in 100ul and fragmented using Bioruptor ultrasonicator (Diagenode) with 30s on/off for 30 cycles. m^{6}A-immunoprecipitation (m^{6}A-IP) and library preparation were performed using EpiMark N6-Methyladenosine enrichment kit (NEB, USA). Input and RNA eluted from m^{6}A-IP were used to prepare libraries with KAPA mRNA Hyper Kit (patient islets samples).

In the samples from EndoC-βH1 cells and mouse islets, we sequenced three replicates for each experimental group. Total RNA was purified using Trizol according to the manufacturer's instruction. Four μg of sonicated total RNA were used for m^{6}A-IP and library were constructed using Takara Pico-Input Strand-Specific Total RNA-seq for Illumina.

All sequencing was performed on Illumina HiSeq 4000 according to the manufacturer's instructions. Approximately 30 million single-end 50-bp reads were generated for each sample.

Data processing and peak calling for m^{6}A sequencing

Cutadapt v1.16[38] was used to remove the first 4 nucleotides of the libraries prepared using "Takara Pico-Input Strand-Specific Total RNA-seq for Illumina". For both m^{6}A-IP and input, reads were aligned to reference genome hg38 using Hisat2 v2.1.0[39] with parameter -k 1. Refseq gene annotation was downloaded from USCS. On average, we obtained 21 million reads quantified on annotated exons.

m^{6}A peak calling for patient samples was performed using R package exomePeak[40]. Homer v4.9.1[41] was used to search for the enriched motif in m^{6}A peak region where the random peaks of 200-bp on human transcriptome were used as background sequence for motif discovery. m^{6}A peak distribution on the metagene was plotted by R package Guitar[42].

Differential expression analysis

The input library of m^{6}A sequencing is essentially an mRNA sequencing library. Thus, we performed gene level differential expression analysis using the input libraries. Specifically, aligned sequencing reads were quantified by Rsubread[43] to obtain gene by sample count matrix. R package DESeq2[44] was used to test for differential expression where sequencing batch, gender, and age were included as covariates. For patient samples, since there are only 69 differentially expressed genes at FDR<0.1 cut-off, we used a less stringent cut off p-value<0.01 to select differential genes for pathway/GO enrichment analysis. ConsensuspathDB[45] was used to perform enrichment analysis. For METTL3 and METTL14 knockdown in EndoC-βH1 cell line, significant differentially expressed genes were selected at adjusted p-value (FDR) cutoff of 0.10.

Differential methylation analysis for m^{6}A sequencing

Differential analysis of m^{6}A methylation for patient samples was performed using R package RADAR (manuscript submitted). Briefly, we divided concatenated exons into 50bp-size consecutive bins and quantified the number of read in each bin. To normalize the Input library size, we used the median-of-ratios method implemented in DESeq2 on gene-level read count. We then used the normalized input to divide IP read count to obtain estimated enrichment for each bin. A size factor for each sample was calculated from the estimated enrichment by the median-of-ratios method, which was then used to account for the IP efficiency and library size. Then the normalized IP read count were further divided by the gene-wise size factor proportional to normalized input read count to account for the pre-IP gene expression level variation for the post-IP data. The normalized and adjusted IP read count were further filtered for bins with read count no less than 15 before testing for differential methylation. To summarize and visualize the m^{6}A methylome data, we performed PCA analysis on the IP read counts that have been adjusted for expression level variation to reduce the dimension of the data and showed the first two principal components in the PCA plot. Specifically, we applied the singular value decomposition approach implemented in R function *prcomp()* on the log-transformed m^{6}A-IP data. The first two PCs were plotted against each other in the PCA plot where each sample was color labeled by predictor variable (disease condition) or covariates (batch, age, sex, etc.).

To make the inferential test, we modeled preprocessed IP read count Y_i in the i th bin by a Poisson distribution (equation 1).

$$\begin{aligned} \mathrm{Y}_i &\sim Poi\left(\lambda_i\right) \\ \log\left(\lambda_i\right) &= \mu_1 + \mathrm{X_i}\beta + e_i \end{aligned} \qquad \text{Equation 1:}$$

We assume a random effect $\mathrm{e}_i \in \log Gamma(\psi, \psi)$, with scale parameter ψ and mean equal to 1. Xi is the design matrix including predictor variable and covariates (batch and gender). Finally, at a FDR cut off of 0.05 we merged all connected significant bins and reported the genomic location of differential m^{6}A peaks.

For the knock-down experiment in EndoC-βH1 cell lines where the sample size is small, R package QNB[44] was used to test for differential methylation on peaks called by the Fisher's exact test.

Single-cell variability analysis

The single cell RNA-seq data was downloaded from Sequence Read Archive (SRA BioProject ID PRJNA322072)[4]. Reads were mapped to the human genome by using the star aligner[46] and the mapped reads for each human gene were counted by using subread feature counts[43]. Classification of cell cycle phase and calculation of gene count normalization factors were done by using the R package scran[47]. Cells belonging to G1 and S phase were selected and the normalization factors were obtained by deconvoluting size factors from cell pools. Gene counts were then normalized and transformed into log2-counts per million (logCPM) by using the voom method of the R package limma[48]. The logCPM were further offset to nonzero values by subtracting the minimum logCPM. Asymptotic test for the equality of coefficients of variation of the offset logCPM was done by using the R package cvequality[49].

We stratified genes by whether the genes carry m^6A modification and compared the variability of gene expression at the single-cell level. Specifically, we define m^6A genes as having a peak called in at least 7 out of 15 samples and non-m^6A genes as none m^6A-peak called in any sample.

Phospho-antibody Microarrays

Islets from 6 week-old male control and M14KO mice were culture for 6h in complete media containing 10% FBS, hand-picked washed 2 times with ice-cold DPBS and pelleted. To perform the Kinex™ KAM-1325 antibody microarray analyses, protein lysates from 200 size-matched islets from each sample (4 control pools and 2 M14KO pools) were covalently labeled with biotin. Free biotin molecules were then removed at the completion of labeling reactions by gel filtration. After blocking non-specific binding sites on the array, an incubation chamber was mounted onto the microarray to permit the loading of 2 samples side by side on the same chip. Following sample incubation, unbound proteins were washed away and the array was then probed with an anti-biotin antibody that is labeled with a proprietary fluorescent dye combination. Each array produced a pair of 16-bit images, which were captured with a Perkin-Elmer ScanArray Reader laser array scanner (Waltham, MA). Signal quantification was performed with ImaGene 9.0 from BioDiscovery (El Segundo, CA) with predetermined settings for spot segmentation and background correction. For normalized phosphosite/protein differential abundance, we used limma, an R package that powers differential expression analyses[48]. We adjusted for the batch effects and performed moderated t-tests between M14KO versus control.

LC-MS/MS quantification of m^6A

We first purified mRNA by two rounds of polyA selection. Fifty ng of purified mRNA were subject to digestion by nuclease P1 (Sigma #N8630–1VL) at 42 degrees for 2 hours followed by phosphatase treatment using FastAP Thermosensitive Alkaline Phosphatase (ThermoFisher #EF0651) at 37 degrees for 1 hour. The digested nucleotides were then

analyzed by ruling through a C18 reverse phase column on HPLC (Agilent) and quantified by triple quad MS/MS system (Sciex).

Pathway enrichment analysis

Pathway and GO enrichment analysis were performed using ConsensusPathDB using default settings[45]. GO terms tree were constructed using Cytoscape's BINGO plugin[50]. Protein-protein functional networks were constructed using STRING using default settings[26].

Study Approval

All animal experiments were conducted in accordance with the Association for Assessment and Accreditation of Laboratory Animal Care. All protocols were approved by the Institutional Animal Care and Use Committee of the Joslin Diabetes Center in accordance with NIH guidelines. All human studies and protocols used were approved by the Joslin Diabetes Center's Committee on Human Studies (CHS#5–05). Formal consent from human islet donors was not required because samples were discarded islets from de-identified humans.

DATA AVAIABILITY

m^6A-sequencing and RNA-sequencing data in human islets have been deposited with the National Center for Biotechnology Information Gene Expression Omnibus under accession code GSE120024. m^6A-sequencing and RNA-sequencing data in EndoC-βH1 cells have been deposited under accession code GSE132306. RNA-sequencing in mouse FACS-sorted β-cells have been deposited under the accession code GSE132306. Phospho-antibody microarrays data performed in mouse whole islets have been deposited under the accession code GSE132111. The data that supports the findings of this study are available from the corresponding author upon reasonable request. R package RADAR code is available upon request.

Supplementary Material

Refer to Web version on PubMed Central for supplementary material.

ACKNOWLEDGMENTS

We thank the Joslin Islet Isolation Core, Joslin Bioinformatics Core and Joslin Advanced Microscopy Core (P30 DK36836). This work is supported by NIH grants R01 DK67536 (R.N.K.), UC4 DK116278 (R.N.K. and C.H.) and RM1 HG008935 (C.H.). R.N.K. acknowledges support from the Margaret A. Congleton Endowed Chair and C.H. is a Howard Hughes Medical Institute Investigator. We would like to sincerely thank the families of the human islet donors.

References

1. De Jesus DF & Kulkarni RN Epigenetic modifiers of islet function and mass. Trends in Endocrinology & Metabolism 25, 628–636, doi:10.1016/j.tem.2014.08.006 (2014). [PubMed: 25246382]
2. Frye M, Harada BT, Behm M & He C RNA modifications modulate gene expression during development. Science 361, 1346–1349, doi:10.1126/science.aau1646 (2018). [PubMed: 30262497]

3. Taneera J et al. Silencing of the FTO gene inhibits insulin secretion: An in vitro study using GRINCH cells. Molecular and Cellular Endocrinology 472, 10–17, doi:10.1016/j.mce.2018.06.003 (2018). [PubMed: 29890211]
4. Xin Y et al. RNA Sequencing of Single Human Islet Cells Reveals Type 2 Diabetes Genes. Cell Metabolism 24, 608–615, doi:10.1016/j.cmet.2016.08.018 (2016). [PubMed: 27667665]
5. Wang X et al. N6-methyladenosine-dependent regulation of messenger RNA stability. Nature 505, 117, doi:10.1038/nature12730 (2013). [PubMed: 24284625]
6. Fadista J et al. Global genomic and transcriptomic analysis of human pancreatic islets reveals novel genes influencing glucose metabolism. Proceedings of the National Academy of Sciences 111, 13924–13929, doi:10.1073/pnas.1402665111 (2014).
7. Gromada J, Chabosseau P & Rutter GA The α-cell in diabetes mellitus. Nature Reviews Endocrinology 14, 694–704, doi:10.1038/s41574-018-0097-y (2018).
8. Diedisheim M et al. Modeling human pancreatic beta cell dedifferentiation. Molecular Metabolism 10, 74–86, doi:10.1016/j.molmet.2018.02.002 (2018). [PubMed: 29472102]
9. Laukkanen O et al. Polymorphisms in the SLC2A2 (GLUT2) gene are associated with the conversion from impaired glucose tolerance to type 2 diabetes: the Finnish Diabetes Prevention Study. The Finnish Diabetes Prevention Study 54, 2256–2260, doi:10.2337/diabetes.54.7.2256 (2005).
10. Wang Y et al. N6-methyladenosine RNA modification regulates embryonic neural stem cell self-renewal through histone modifications. Nature Neuroscience 21, 195–206, doi:10.1038/s41593-017-0057-1 (2018). [PubMed: 29335608]
11. Kulkarni RN et al. PDX-1 haploinsufficiency limits the compensatory islet hyperplasia that occurs in response to insulin resistance. The Journal of Clinical Investigation 114, 828–836, doi:10.1172/jci21845 (2004). [PubMed: 15372107]
12. Stoffers DA, Zinkin NT, Stanojevic V, Clarke WL & Habener JF Pancreatic agenesis attributable to a single nucleotide deletion in the human IPF1 gene coding sequence. Nature Genetics 15, 106, doi:10.1038/ng0197-106 (1997). [PubMed: 8988180]
13. Guo S et al. Inactivation of specific β cell transcription factors in type 2 diabetes. The Journal of Clinical Investigation 123, 3305–3316, doi:10.1172/jci65390 (2013). [PubMed: 23863625]
14. Humphrey RK, Yu S-M, Flores LE & Jhala US Glucose Regulates Steady-state Levels of PDX1 via the Reciprocal Actions of GSK3 and AKT Kinases. Journal of Biological Chemistry 285, 3406–3416, doi:10.1074/jbc.M109.006734 (2010). [PubMed: 19833727]
15. Elghazi L & Bernal-Mizrachi E Akt and PTEN: beta-cell mass and pancreas plasticity. Trends in Endocrinology &Metabolism 20, 243–251, doi:10.1016/j.tem.2009.03.002 (2009). [PubMed: 19541499]
16. Ravassard P et al. A genetically engineered human pancreatic β cell line exhibiting glucose-inducible insulin secretion. The Journal of Clinical Investigation 121, 3589–3597, doi:10.1172/jci58447 (2011). [PubMed: 21865645]
17. Tsonkova VG et al. The EndoC-βH1 cell line is a valid model of human beta cells and applicable for screenings to identify novel drug target candidates. Molecular Metabolism 8, 144–157, doi:10.1016/j.molmet.2017.12.007 (2018). [PubMed: 29307512]
18. Boucher M-J, Selander L, Carlsson L & Edlund H Phosphorylation Marks IPF1/PDX1 Protein for Degradation by Glycogen Synthase Kinase 3-dependent Mechanisms. Journal of Biological Chemistry 281, 6395–6403, doi:10.1074/jbc.M511597200 (2006). [PubMed: 16407209]
19. Wang X et al. N6-methyladenosine Modulates Messenger RNA Translation Efficiency. Cell 161, 1388–1399, doi:10.1016/j.cell.2015.05.014 (2015). [PubMed: 26046440]
20. Tang L et al. Suppression of Sirtuin-1 Increases IL-6 Expression by Activation of the Akt Pathway During Allergic Asthma. Cellular Physiology and Biochemistry 43, 1950–1960, doi:10.1159/000484119 (2017). [PubMed: 29055943]
21. Lu H, Koshkin V, Allister EM, Gyulkhandanyan AV & Wheeler MB Molecular and Metabolic Evidence for Mitochondrial Defects Associated With β-Cell Dysfunction in a Mouse Model of Type 2 Diabetes. Diabetes 59, 448–459, doi:10.2337/db09-0129 (2010). [PubMed: 19903739]

22. Smelt MJ, Faas MM, de Haan BJ & de Vos P Pancreatic Beta-Cell Purification by Altering FAD and NAD(P)H Metabolism. Experimental Diabetes Research 2008, 11, doi:10.1155/2008/165360 (2008).

23. Cook RS et al. ErbB3 ablation impairs PI3K/Akt-dependent mammary tumorigenesis. Cancer research 71, 3941–3951, doi:10.1158/0008-5472.can-10-3775 (2011). [PubMed: 21482676]

24. Rabinovsky R et al. p85 Associates with Unphosphorylated PTEN and the PTEN-Associated Complex. Molecular and cellular biology 29, 5377–5388, doi:10.1128/mcb.01649-08 (2009). [PubMed: 19635806]

25. Vazquez F, Ramaswamy S, Nakamura N & Sellers WR Phosphorylation of the PTEN tail regulates protein stability and function. Molecular and cellular biology 20, 5010–5018 (2000). [PubMed: 10866658]

26. Snel B et al. STRING: known and predicted protein–protein associations, integrated and transferred across organisms. Nucleic Acids Research 33, D433–D437, doi:10.1093/nar/gki005 (2005). [PubMed: 15608232]

27. Weng H et al. METTL14 Inhibits Hematopoietic Stem/Progenitor Differentiation and Promotes Leukemogenesis via mRNA m6A Modification. Cell stem cell 22, 191–205.e199, doi:10.1016/j.stem.2017.11.016 (2018). [PubMed: 29290617]

28. Yoon K-J et al. Temporal Control of Mammalian Cortical Neurogenesis by m6A Methylation. Cell 171, 877–889.e817, doi:10.1016/j.cell.2017.09.003 (2017). [PubMed: 28965759]

29. Liu J et al. m6A mRNA methylation regulates AKT activity to promote the proliferation and tumorigenicity of endometrial cancer. Nature Cell Biology 20, 1074–1083, doi:10.1038/s41556-018-0174-4 (2018). [PubMed: 30154548]

30. Min K-W et al. Profiling of m6A RNA modifications identified an age-associated regulation of AGO2 mRNA stability. Aging Cell 17, e12753, doi:doi:10.1111/acel.12753 (2018). [PubMed: 29573145]

31. Thorens B et al. Ins1Cre knock-in mice for beta cell-specific gene recombination. Diabetologia 58, 558–565, doi:10.1007/s00125-014-3468-5 (2015). [PubMed: 25500700]

32. El Ouaamari A et al. Compensatory Islet Response to Insulin Resistance Revealed by Quantitative Proteomics. Journal of Proteome Research, doi:10.1021/acs.jproteome.5b00587 (2015).

33. Dirice E et al. Soluble Factors Secreted by T Cells Promote β-Cell Proliferation. Diabetes 63, 188–202, doi:10.2337/db13-0204 (2014). [PubMed: 24089508]

34. El Ouaamari A et al. SerpinB1 Promotes Pancreatic β Cell Proliferation. Cell Metabolism 23, 194–205, doi:10.1016/j.cmet.2015.12.001 (2016). [PubMed: 26701651]

35. Dirice E et al. Increased β-cell proliferation before immune cell invasion prevents progression of type 1 diabetes. Nature Metabolism 1, 509–518, doi:10.1038/s42255-019-0061-8 (2019).

36. Kulkarni RN et al. Tissue-Specific Knockout of the Insulin Receptor in Pancreatic β Cells Creates an Insulin Secretory Defect Similar to that in Type 2 Diabetes. Cell 96, 329–339, doi:10.1016/s0092-8674(00)80546-2 (1999). [PubMed: 10025399]

37. Kahraman S, Dirice E, De Jesus DF, Hu J & Kulkarni RN Maternal insulin resistance and transient hyperglycemia impact the metabolic and endocrine phenotypes of offspring. American journal of physiology. Endocrinology and metabolism 307, E906–918, doi:10.1152/ajpendo.00210.2014 (2014). [PubMed: 25249504]

38. Martin M Cutadapt removes adapter sequences from high-throughput sequencing reads. 2011 17, 3, doi:10.14806/ej.17.1.200 (2011).

39. Kim D, Langmead B & Salzberg SL HISAT: a fast spliced aligner with low memory requirements. Nature methods 12, 357–360, doi:10.1038/nmeth.3317 (2015). [PubMed: 25751142]

40. Meng J, Cui X, Rao MK, Chen Y & Huang Y Exome-based analysis for RNA epigenome sequencing data. Bioinformatics 29, 1565–1567, doi:10.1093/bioinformatics/btt171 (2013). [PubMed: 23589649]

41. Heinz S et al. Simple combinations of lineage-determining transcription factors prime cis-regulatory elements required for macrophage and B cell identities. Mol Cell 38, 576–589, doi:10.1016/j.molcel.2010.05.004 (2010). [PubMed: 20513432]

42. Cui X et al. Guitar: An R/Bioconductor Package for Gene Annotation Guided Transcriptomic Analysis of RNA-Related Genomic Features. Biomed Res Int 2016, 8367534, doi: 10.1155/2016/8367534 (2016). [PubMed: 27239475]

43. Liao Y, Smyth GK & Shi W The Subread aligner: fast, accurate and scalable read mapping by seed-and-vote. Nucleic Acids Research 41, e108–e108, doi:10.1093/nar/gkt214 (2013). [PubMed: 23558742]

44. Love MI, Huber W & Anders S Moderated estimation of fold change and dispersion for RNA-seq data with DESeq2. Genome Biol 15, 550, doi:10.1186/s13059-014-0550-8 (2014). [PubMed: 25516281]

45. Herwig R, Hardt C, Lienhard M & Kamburov A Analyzing and interpreting genome data at the network level with ConsensusPathDB. Nature Protocols 11, 1889, doi:10.1038/nprot.2016.117 (2016). [PubMed: 27606777]

46. Dobin A et al. STAR: ultrafast universal RNA-seq aligner. Bioinformatics 29, 15–21, doi:10.1093/bioinformatics/bts635 (2013). [PubMed: 23104886]

47. Scialdone A et al. Computational assignment of cell-cycle stage from single-cell transcriptome data. Methods 85, 54–61, doi:10.1016/j.ymeth.2015.06.021 (2015). [PubMed: 26142758]

48. Law CW, Chen Y, Shi W & Smyth GK voom: Precision weights unlock linear model analysis tools for RNA-seq read counts. Genome Biol 15, R29, doi:10.1186/gb-2014-15-2-r29 (2014). [PubMed: 24485249]

49. Krishnamoorthy K & Lee M Improved tests for the equality of normal coefficients of variation. Computational Statistics 29, 215–232, doi:10.1007/s00180-013-0445-2 (2014).

50. Maere S, Heymans K & Kuiper M BiNGO: a Cytoscape plugin to assess overrepresentation of Gene Ontology categories in Biological Networks. Bioinformatics 21, 3448–3449, doi:10.1093/bioinformatics/bti551 (2005). [PubMed: 15972284]

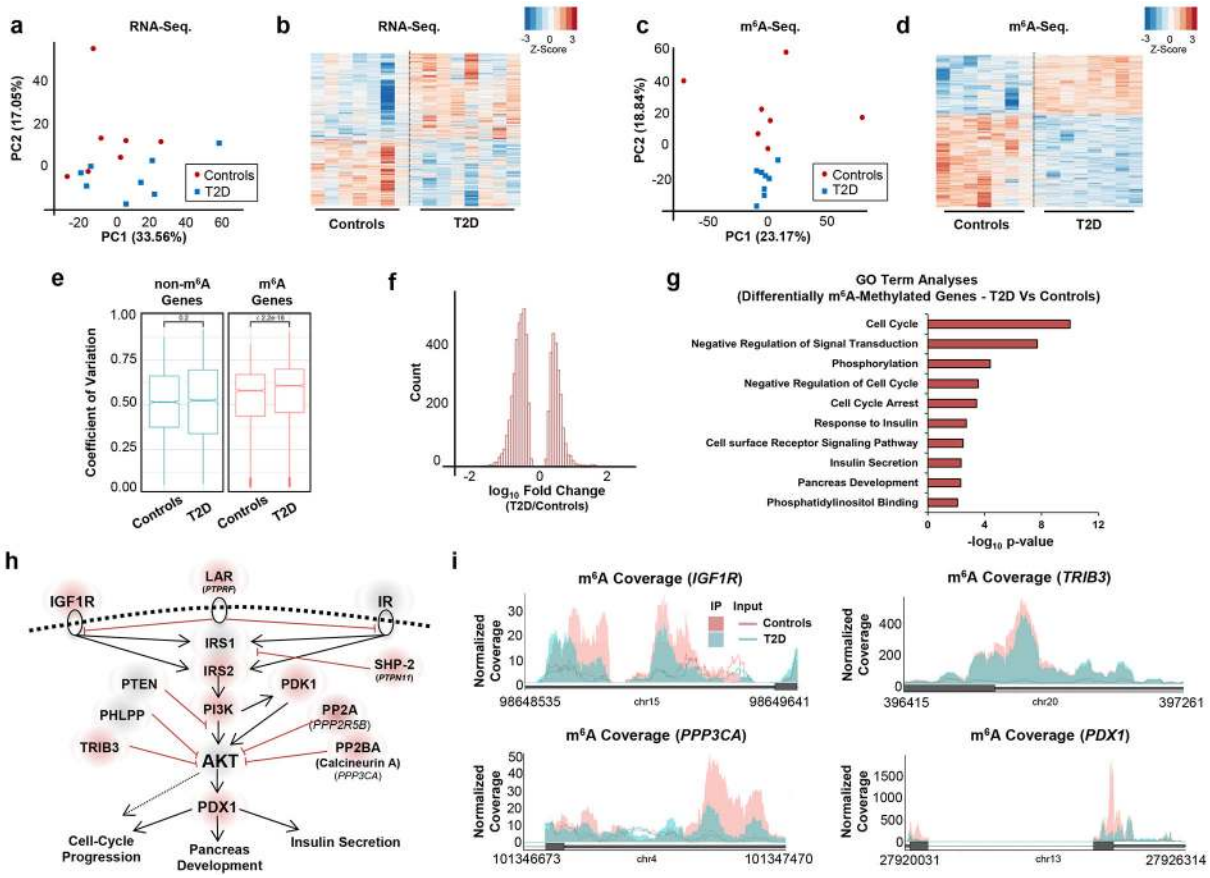

Figure 1: RNA N6-methyladenosine sequencing reveals a homogeneous m^{6}A decoration in human type 2 diabetic islets.

a, PCA plot of RNA-sequencing after regressing out batch, gender and age in Controls (red dots, n=7 independent biological samples) and type 2 diabetic islets (T2D, blue squares, n=8 independent biological samples). **b**, Heat-map visualization of differential expressed genes in Controls versus T2D islets. **c**, PCA plot of m^{6}A-sequencing after regressing out the batch and gender effects in Controls (red dots, n=7 independent biological samples) and T2D islets (T2D, blue squares, n=8 independent biological samples). **d**, Heat-map visualization of differential methylated loci in Controls versus T2D islets. **e**, The gene expression variability of β-cells represented by the coefficient of variation from single-cell RNA sequencing data (GSE81608) in human dispersed islets comparing Controls (n=12 independent biological samples) and T2D patients (n=6 independent biological samples). The stratification of m^{6}A-modified vs. non-m^{6}A-modified gene is based on our patient m^{6}A-sequencing data. Box plot shows the median, box edges show first and third quartiles and whiskers show the minimum and maximum. *P*-values were calculated using Mann-Whitney-Wilcoxon test. **f**, Histogram of log-fold change showing the distribution of differential m^{6}A loci fold changes from Controls versus T2D. **g**, Gene-ontology (GO) analyses of differently m^{6}A-methylated genes in T2D (=8 independent biological samples) versus Control (n=7 independent biological samples) islets. *P*-values were calculated according to the hypergeometric test based on the number of physical entities present in both the predefined set and user-specified list of physical entities. **h**, Representation of Insulin/IGF1 pathway and induction of PDX1

expression based on KEEG and Wikipathway annotations depicting several m^6A hypomethylated genes (red shade) and unchanged genes (grey shade) in T2D as compared to Controls (genes filtered for FDR<0.05). **I**, Coverage plots of m^6A peaks in PDX1 gene comparing T2D (=8 independent biological samples) versus Controls (n=7 independent biological samples). Plotted coverages are the median of the n replicates presented.

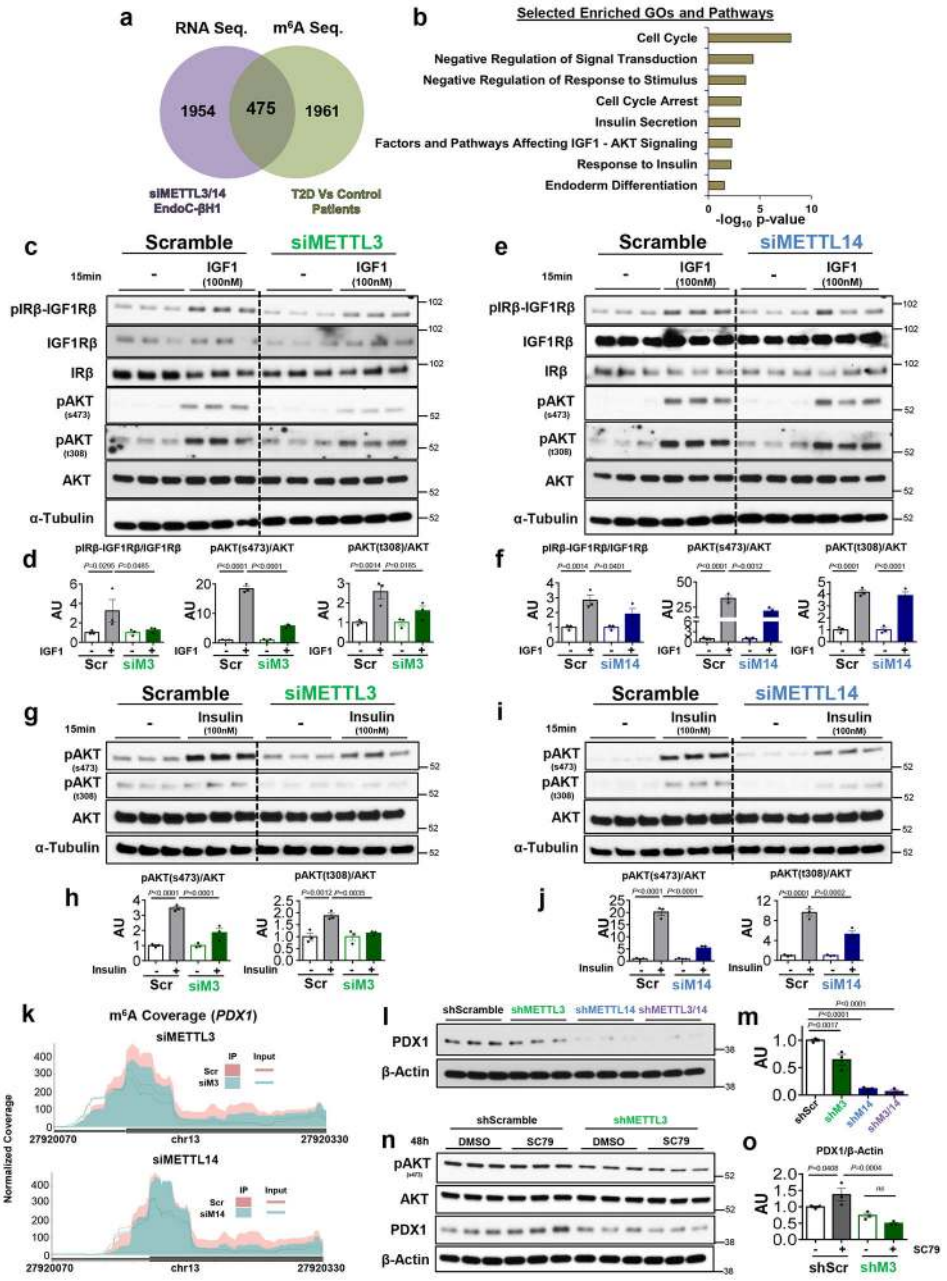

Figure 2: m^{6}A controls PDX1 expression and modulates Insulin/IGF1-mediated AKT phosphorylation.

a, Venn diagram representation of the intersection between differently methylated genes in T2D human islets and differentially expressed genes in METTL3 KD and METTL14 KD in EndoC-βH1 (Human islets: Controls, n=7 independent biological samples; T2D, n=8 independent biological samples. EndoC-βH1 cells: n=3 independent experiments/group). Statistical analyses was performed using Benjamini-Hochberg procedure and genes were filtered for FDR<0.10. **b**, Enriched-GO and pathway analyses of intersected genes (Human islets: Controls, n=7 independent biological samples; T2D, n=8 independent biological samples. EndoC-βH1 cells: n=3 independent experiments/group). *P*-values were calculated

according to the hypergeometric test based on the number of physical entities present in both the predefined set and user-specified list of physical entities. **c**, Western-blot analyses of indicated proteins after IGF1 stimulation in METTL3 KD in EndoC-βH1 cells (n=3 independent experiments/group/condition). **d**, Protein quantification of indicated protein after IGF1 stimulation in METTL3 KD. **e**, Western-blot analyses of indicated proteins after IGF1 stimulation in METTL14 KD EndoC-βH1 cells (n=3 independent experiments/group/condition). **f**, Protein quantification of indicated proteins after IGF1 stimulation in METTL14 KD. **g**, Western-blot analyses of indicated proteins after insulin stimulation in METTL3 KD (n=3 independent experiments/group/condition). **h**, Protein quantification of indicated protein after insulin stimulation in METTL3 KD. **i**, Western-blot analyses of indicated proteins after insulin stimulation in METTL14 KD (n=3 independent experiments/group/condition). **j**, Protein quantification of indicated proteins after insulin stimulation in METTL14 KD. **k**, Coverage plot of m^6A peaks in PDX1 gene depicting hypomethylation after METTL3 or METTL14 KD in EndoC-βH1 (n=3 independent experiments/group, FDR<0.05). **l**, Western-blot analyses of PDX1 protein levels in stable METTL3 KD, METTL14 KD or (METTL3 + METTL14) KD (n=3 independent experiments/group). **m**, PDX1 protein quantification. **n**, Western-blot analyses of indicated proteins after DMSO or SC79 stimulation in METTL3 KD for 48h (n=3 independent experiments/group/condition). **o**, PDX1 protein quantifications. Data are represented as mean ± SEM. Statistical analyses by Two-way ANOVA with Fisher's LSD test (in **d**,**f**,**h**,**j**,**m** and **o**).

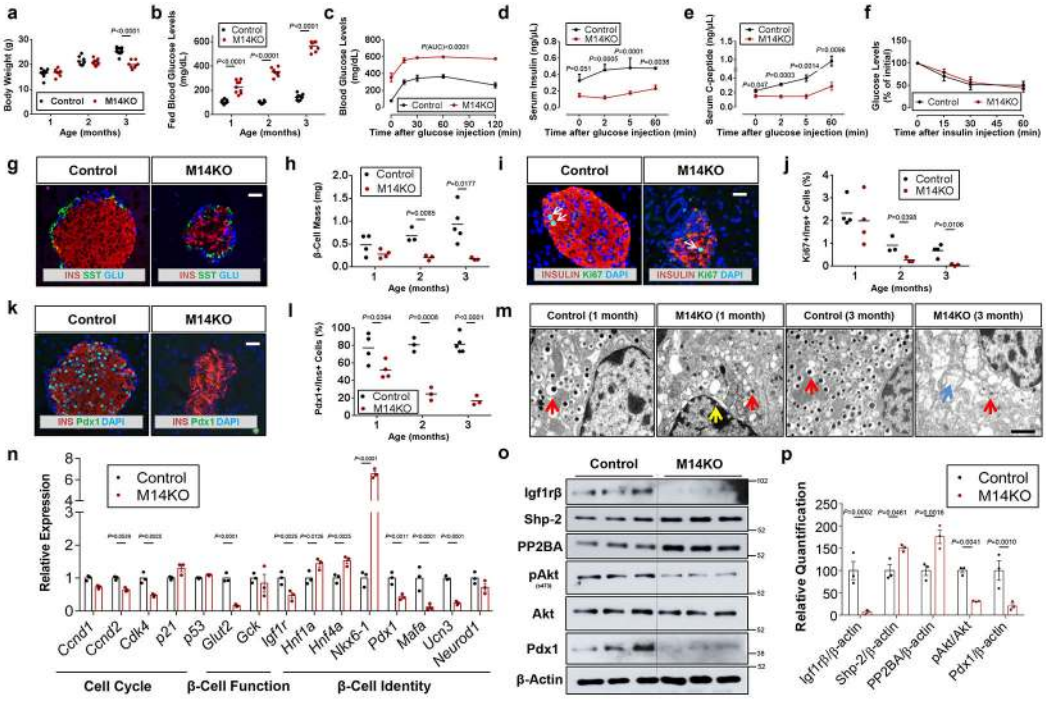

Figure 3: β-cell specific Mettl14 knock-out (KO) results in early diabetes and mortality secondary to decreased Pdx-1 expression and decreased phosphorylation of AKT.

a, Body weight trajectories of Controls (black dots) and Mettl14 KO mice (M14KO) (red dots) (1 month: n=9 independent biological samples in Controls and M14KO; 2 months: n=8 independent biological samples in Controls and n=9 independent biological samples in M14KO; 3 months: n=10 independent biological samples in Controls and n=8 independent biological samples in M14KO). **b**, Random-fed blood glucose levels in Controls and M14KO (1 month: n=9 independent biological samples in Controls and M14KO; 2 months: n=8 independent biological samples in Controls and M14KO; 3 months: n=10 independent biological samples in Controls and n=8 independent biological samples in M14KO). **c**, Blood glucose levels after a glucose tolerance test in 2 month-old Controls (black line) and M14KO (red line) (n=6 animals/group). **d**, Serum insulin levels after an *in vivo* glucose-stimulated insulin secretion assay in 2 month old Controls (black line) and M14KO (red line) (n=4 animals/group). **e**, Serum C-peptide levels after an *in vivo* glucose-stimulated insulin secretion assay in 2 month-old Controls (black line) and M14KO (red line) (n=4 animals/group). **f**, Blood glucose levels after an insulin tolerance test in 2 month-old Controls (black line) and M14KO (red line) (n=6 animals/group). **g**, Representative pictures of immunofluorescence staining of insulin (red), somatostatin (green) and glucagon (blue) in pancreas sections from Controls and M14KO (n=3–5 animals/group). **h**, β-cell mass quantification in Controls and M14KO (1 month: n=4 independent biological samples in Controls and M14KO; 2 months: n=3 independent biological samples in Controls and M14KO; 3 months: n=5 independent biological samples in Controls and n=3 independent biological samples in M14KO). **i**, Representative pictures of immunofluorescence staining of Ki67 (green), insulin (red) and DAPI (blue) in pancreas sections from Controls and M14KO mice (n=3–5 animals/group). **j**, β-cell proliferation quantification in Controls and M14KO mice (1 month: n=4 independent biological samples in Controls and M14KO; 2

months: n=3 independent biological samples in Controls and M14KO; 3 months: n=5 independent biological samples in Controls and n=3 independent biological samples in M14KO). **k**, Representative pictures of immunofluorescence staining of Pdx1 (green), insulin (red) and DAPI (blue) in pancreas sections from Controls and M14KO (n=3–5 animals/group). **l**, Quantification of Pdx1+/Insulin+ cells in pancreas sections from Controls and M14KO (1 month: n=4 independent biological samples in Controls and M14KO; 2 months: n=3 independent biological samples in Controls and M14KO; 3 months: n=5 independent biological samples in Controls and n=3 independent biological samples in M14KO). **m**, Representative images of electron microscopic analyses of islet cell ultrastructure in 1 and 3 month-old Controls and M14KO (n=3 animals/group). Red arrows point to insulin granules that are degranulated in M14KO compared to Controls. Yellow arrow refers to the presence of nuclear membrane swelling in M14KO as compared to Controls (left two panels). Blue arrow points to enlarged mitochondria in M14KO as compared to Controls (right two panels). **n**, qRT-PCR analyses of the cell cycle, function and identity genes in whole islets isolated from 2 month old Controls (n=3 animals) and M14KO (n=6 animals). **o**, Western Blot analyses of indicated proteins in whole islets isolated from 2 months old Controls (n=3 pools, 2 animals/pool) and M14KO (n=3 pools, 4 animals/pool). **p**, Quantifications of indicated proteins. Data are represented as mean ± SEM. In all panels statistical analyses were performed by two-sided unpaired multiple t-tests and corrected for multiple comparisons using the Holm-Sidak method. Scale bar = 100 μm.

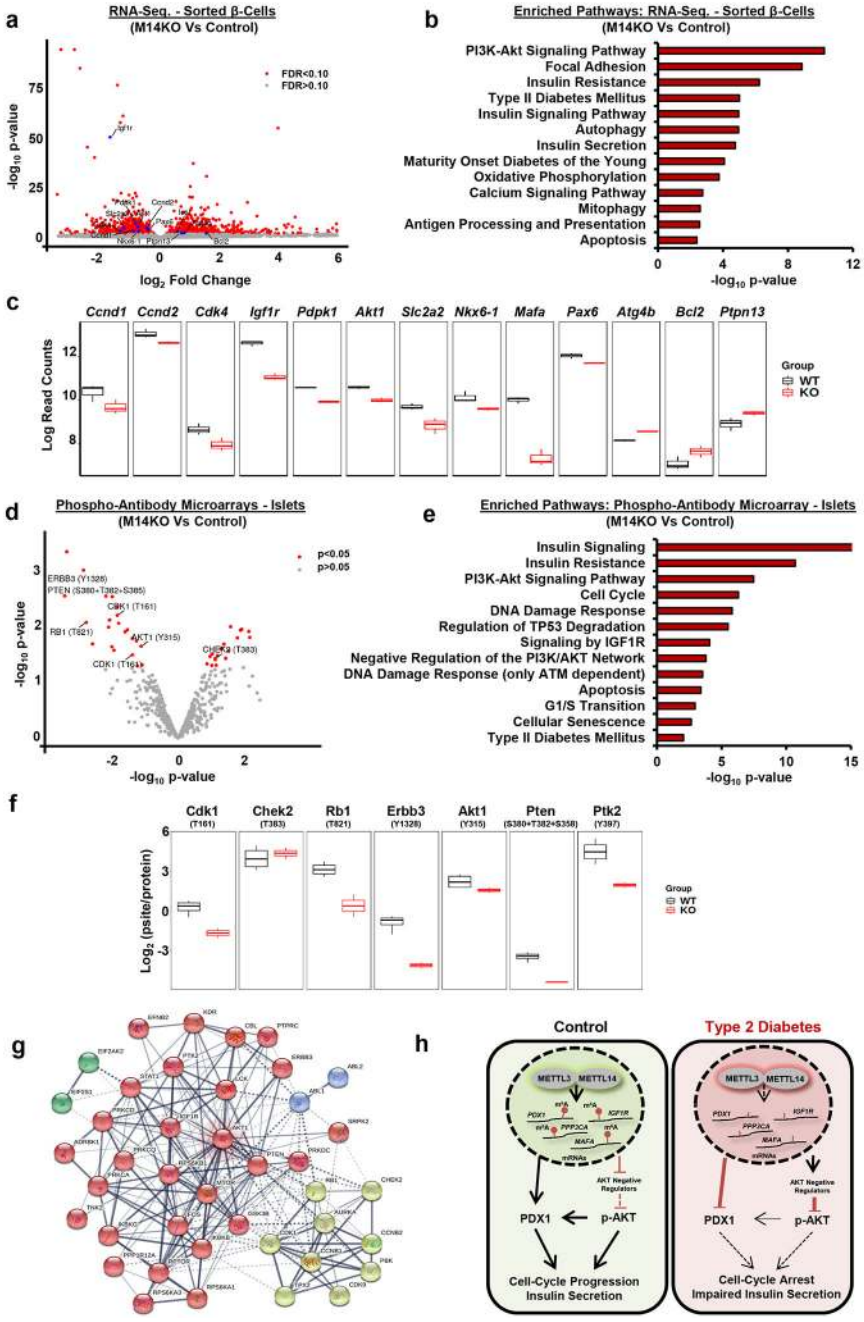

Figure 4: Functional protein-protein interaction network analyses reveal the central role of AKT in controlling the effects of Mettl14 ablation in β-cells.

a, Volcano-plot representation of differentially expressed genes by RNA-sequencing in FACS-sorted β-cells from M14KO compared to Controls (Controls, n=4 pools, 2 animals/pool; M14KO, n=4 pools, 4 animals/pool). Statistical analyses was performed using Benjamini-Hochberg procedure and genes were filtered for FDR<0.10. **b**, Enriched pathway analyses of significantly altered genes between M14KO and Controls (Controls, n=4 pools, 2 animals/pool; M14KO, n=4 pools, 4 animals/pool) (genes filtered for FDR<0.10) (p-values were calculated according to the hypergeometric test based on the number of physical

entities present in both the predefined set and user-specified list of physical entities). **c**, Representation of altered genes in β-cells from M14KO compared to Controls (Controls, n=4 pools, 2 animals/pool; M14KO, n=4 pools, 4 animals/pool). Box plot shows the median, box edges show first and third quartiles and whiskers show the minimum and maximum. **d**, Volcano-plot representation of altered phosphosites by phospho-antibody microarrays in whole islets from M14KO compared to Controls (Controls, n=4 animals; M14KO, n=2 pools, 4 animals/pool). Statistical analyses were performed by using moderated t-tests with linear models for microarray data. **e**, Enriched pathway analyses of significantly altered phosphosites between M14KO and Controls (Controls, n=4 animals; M14KO, n=2 pools, 4 animals/pool) (genes filtered for $p<0.05$). **f**, Representation of altered phosphosites in M14KO islets compared to Controls (Controls, n=4 animals; M14KO, n=2 pools, 4 animals/pool). Box plot shows the median, box edges show first and third quartiles and whiskers show the minimum and maximum. **g**, Functional protein-protein interaction network of significantly altered phosphosites in M14KO compared to Controls. Different colors represent network nodes. **h**, Model depicting the effect of decreased expression of m^6A modulators in type 2 diabetes: a) induces a generalized state of hypomethylation and downregulation of PDX1 and, b) increases expression of negative regulators of AKT, leading to decreased phosphorylation of AKT and consequent cell-cycle arrest and impaired insulin secretion.